Compact fourth-order finite difference method for solving differential equations

P. B. Wilkinson,[1] T. M. Fromhold,[1] C. R. Tench,[1] R. P. Taylor,[2] and A. P. Micolich[2]
[1]*School of Physics and Astronomy, University of Nottingham, Nottingham, NG7 2RD, United Kingdom*
[2]*Department of Physics, University of Oregon, Eugene, Oregon 97403-1274*
(Received 27 March 2001; published 17 September 2001)

We present a fourth-order finite difference (FD) method for solving two-dimensional partial differential equations. The FD operator uses a compact nine-point stencil on a regular square grid. Despite the regular grid, Dirichlet boundary conditions can be applied on an arbitrarily shaped boundary without resorting to the usual stepped approximation. We demonstrate the superior convergence of the method over second-order techniques by solving the Schrödinger equation for an electron in a semiconductor quantum dot with a smoothly varying potential which generates classically chaotic dynamics.

DOI: 10.1103/PhysRevE.64.047701 PACS number(s): 02.70.Bf, 02.30.Jr, 05.45.Mt

Finite difference (FD) methods for the numerical solution of partial differential equations (PDEs) approximate continuous derivatives by discrete difference operators. These operators are obtained from Taylor expansions of the solution at discrete points on a grid. They have a certain order of accuracy, $O(\Delta^2)$ for the simplest method and $O(\Delta^4)$ for more complicated methods, where Δ is the grid spacing. The higher order schemes require far fewer points for numerically accurate solutions. FD methods are called *compact* if the ''stencil'' of grid points used in the difference operator involves only immediate neighbors of the central point.

For two-dimensional (2D) PDEs, $O(\Delta^2)$ methods are compact and allow boundary conditions to be applied easily. Compact $O(\Delta^4)$ methods have been developed for solving the 2D elliptic and Helmholtz PDEs [1,2]. In this paper, we present a *general* compact $O(\Delta^4)$ method in 2D. Dirichlet boundary conditions can be applied along an arbitrary boundary without recourse to the usual stepped approximation. The superior convergence of this $O(\Delta^4)$ method over $O(\Delta^2)$ schemes is demonstrated by solving the 2D Schrödinger equation for an open semiconductor quantum dot with classically chaotic dynamics. We emphasize that the method can be applied to many other 2D PDEs. For example, we have used it to solve the scalar electromagnetic wave equation in a gradient refractive index lens [3].

A second-order FD approximation to the 2D time-independent Schrödinger equation

$$-\frac{\hbar^2\nabla^2}{2m}\psi(x,y)+V(x,y)\psi(x,y)=E\psi(x,y) \tag{1}$$

for the wave function $\psi(x,y)$ of a particle of mass m, energy E, and potential energy $V(x,y)$ can be obtained using the five-point stencil shown as filled circles in Fig. 1. The Taylor expansion

$$\psi_{i+a,j+b}=\psi_{i,j}+\sum_{n=1}^{\infty}\frac{1}{n!}\left(a\Delta\frac{\partial}{\partial x}+b\Delta\frac{\partial}{\partial y}\right)^n\psi_{i,j} \tag{2}$$

is used to derive approximate values of the wave function at the points $(i+1,j)$, $(i-1,j)$, $(i,j+1)$, and $(i,j-1)$. In the $O(\Delta^2)$ approximation, the summation is truncated at $n=2$. The resulting equations show that

$$\frac{\partial^2\psi_{i,j}}{\partial x^2}\approx\frac{\psi_{i+1,j}-2\psi_{i,j}+\psi_{i-1,j}}{\Delta^2} \tag{3}$$

and

$$\frac{\partial^2\psi_{i,j}}{\partial y^2}\approx\frac{\psi_{i,j+1}-2\psi_{i,j}+\psi_{i,j-1}}{\Delta^2}. \tag{4}$$

Substituting Eqs. (3) and (4) into Eq. (1) and applying the resulting FD equation to each of the N grid points in the system gives N simultaneous linear equations. These equations can be written in the form

$$\mathbf{M}\Psi=\mathbf{b}, \tag{5}$$

where the vector Ψ contains the discrete wave function values $\psi_{i,j}$ and the constant vector $\mathbf{b}$ depends on the boundary conditions. The nonzero elements of the coefficient matrix $\mathbf{M}$ form a narrow band about the leading diagonal with bandwidth $W\propto\sqrt{N}$. Keeping the band as narrow as possible is important, as the computational effort required to solve Eq. (5) increases dramatically with increasing W.

The above method can be improved to fourth-order accuracy by using the spatially extended stencil formed by the nine points shown as filled and dotted circles in Fig. 1. Equation (2) is used to derive approximations to the wave function values at the eight points surrounding (i,j) with the summation truncated at $n=4$. The resulting equations give

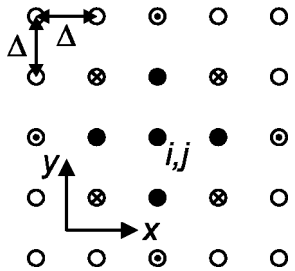

FIG. 1. Stencils used in the second-order (filled circles), fourth-order (filled and dotted circles), and our compact fourth-order (filled and crossed circles) FD methods. Each stencil is centered on point (i,j).

$O(\Delta^4)$ approximations to $\partial^2\psi_{i,j}/\partial x^2$ and $\partial^2\psi_{i,j}/\partial y^2$ in terms of the wave function values on the extended stencil.

While easy to apply and understand, this traditional fourth-order approach has drawbacks. First, Dirichlet boundary conditions can be implemented only with second-order accuracy [4]. More importantly the bandwidth of the matrix is $2W$, double that of the $O(\Delta^2)$ method. This doubles the memory requirements, but *quadruples* the operation count and execution time.

Here we develop an $O(\Delta^4)$ FD method with the same narrow bandwidth as the $O(\Delta^2)$ method. We consider the nine-point stencil shown by filled and crossed circles in Fig. 1. The inclusion of the crossed circle points introduces mixed partial derivatives into the Taylor expansion, which is again truncated at $n=4$. Using Eq. (2) to determine the wave function values at the eight points surrounding (i,j) gives eight independent linear equations of the form

$$\begin{aligned}\psi_{i+a,j+b}-\psi_{i,j}\approx\Delta[a\psi^x+b\psi^y]+\frac{\Delta^2}{2}[a^2\psi^{xx}+2ab\psi^{xy}\\+b^2\psi^{yy}]+\frac{\Delta^3}{6}[a^3\psi^{xxx}+3a^2b\psi^{xxy}\\+3ab^2\psi^{xyy}+b^3\psi^{yyy}]+\frac{\Delta^4}{24}[a^4\psi^{xxxx}\\+4a^3b\psi^{xxxy}+6a^2b^2\psi^{xxyy}+4ab^3\psi^{xyyy}\\+b^4\psi^{yyyy}],\end{aligned}\tag{6}$$

where a and $b=0,\pm1$. These equations involve 14 derivative terms denoted, for example, $\psi^{xxxy}\equiv\partial^4\psi_{i,j}/\partial x^3\partial y$. We generate five more independent equations by repeated differentiation of Eq. (1):

$$V^x\psi_{i,j}=(E-V_{i,j})\psi^x+\frac{\hbar^2}{2m}\psi^{xxx}+\frac{\hbar^2}{2m}\psi^{xyy},\tag{7}$$

$$V^y\psi_{i,j}=(E-V_{i,j})\psi^y+\frac{\hbar^2}{2m}\psi^{yyy}+\frac{\hbar^2}{2m}\psi^{xxy},\tag{8}$$

$$V^{xx}\psi_{i,j}=(E-V_{i,j})\psi^{xx}+\frac{\hbar^2}{2m}\psi^{xxxx}+\frac{\hbar^2}{2m}\psi^{xxyy}-2V^x\psi^x,\tag{9}$$

$$V^{yy}\psi_{i,j}=(E-V_{i,j})\psi^{yy}+\frac{\hbar^2}{2m}\psi^{yyyy}+\frac{\hbar^2}{2m}\psi^{xxyy}-2V^y\psi^y,\tag{10}$$

$$\begin{aligned}V^{xy}\psi_{i,j}=(E-V_{i,j})\psi^{xy}+\frac{\hbar^2}{2m}(\psi^{xxxy}+\psi^{xyyy})-V^x\psi^y\\-V^y\psi^x,\end{aligned}\tag{11}$$

where the derivatives of V (for example, $V^{xy}\equiv\partial^2V_{i,j}/\partial x\partial y$) are known. The coefficients of ψ^{xxxy} and ψ^{xyyy} are equal in Eq. (6) (because either $a=0$, $b=0$, or $|a|=|b|$) and in Eq. (11). Therefore $\psi^{xxxy}+\psi^{xyyy}$ reduces to one independent term. The 13 independent equations involving the 13 independent derivative terms are solved by numerical matrix inversion for each of the N grid points. This gives $O(\Delta^4)$ approximations to $\partial^2\psi_{i,j}/\partial x^2$ and $\partial^2\psi_{i,j}/\partial y^2$ in terms of a weighted sum of the wave function values at the nine points of the compact stencil [5]. Using these expressions to approximate Eq. (1) at each grid point gives a matrix equation like Eq. (5). Typically, the bandwidth of $\mathbf{M}$ using this $O(\Delta^4)$ method is only $W+1$.

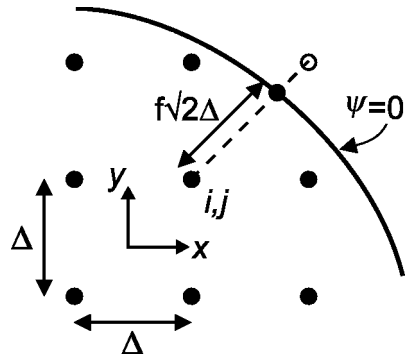

FIG. 2. Example of the compact $O(\Delta^4)$ stencil at a boundary (solid curve). The point on the square stencil lying outside the boundary (open circle) is replaced by a new point (filled circle) at the intersection of the boundary and the dashed line. This new point is at a fraction f of the distance from the center point to the external point.

Where the value of the wave function is known on a boundary (a Dirichlet boundary condition), this information must be included in Eq. (5). To avoid the traditional stepped approximation to a curved boundary [4], we replace each point in the stencil that lies outside the boundary with a new point that lies exactly on it. The new point is placed at the intersection of the boundary and the line connecting the point (i,j) to the external point. This ensures that for external points at the corners of the stencil the x and y displacements from (i,j) are equal, so that the coefficients of ψ^{xxxy} and ψ^{xyyy} in Eq. (6) also remain equal. For example, in Fig. 2 the point $(i+1,j+1)$ (open circle) lies outside a boundary (solid line) on which $\psi=0$. This external point is replaced by a new point (filled circle) which lies on the boundary and on the dashed line at a distance $f\sqrt{2}\Delta$ from the center point, where $0<f<1$. For the external point in Fig. 2, $a=b=1$ in Eq. (6). The new point has $a=b=f$. The known wave function value $\psi_{i+f,j+f}=0$ can then be inserted into Eq. (6). $O(\Delta^4)$ approximations to the derivatives are calculated as before, but using the wave function values on the modified stencil (filled circles in Fig. 2).

We used this method to calculate the transmission properties of semiconductor [6] and optical [3] devices connected to semi-infinite leads. This involves applying Dirichlet boundary conditions at the walls of the device and a mixture of Dirichlet and Neumann boundary conditions at the interface between the device and the lead. Consider the interface at $x=0$ shown schematically in Fig. 3. In the lead, to the left of the interface, an electron moves freely in the semi-infinite x direction, but is confined along y, producing a set of orthonormal quantized modes [6]. The wave function in the lead has the general form

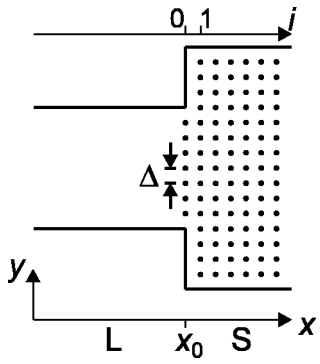

FIG. 3. The interface at $x=x_0$ between the lead (region L, unbounded for $x<x_0$) and the FD solution (region S, bounded at some $x>x_0$).

$$\psi_L(x,y)=A\exp[i\beta_l(x-x_0)]f_l(y)+\sum_{r=1}^{R}B_r \times\exp[-i\beta_r(x-x_0)]f_r(y), \tag{12}$$

where β_p and $f_p(y)$ are the wave number and y dependence of mode p, the incident mode has index l, and the reflected modes have indices $\{r\}$. The wave number is real for propagating modes and imaginary for evanescent modes (which must be included to ensure correct matching of ψ across the interface). The complex coefficients of the incident and reflected modes are A and $\{B_r\}$, respectively. By matching ψ, the wave function on the grid points inside the device, and ψ_L at x_0 we satisfy the Dirichlet boundary condition. For a given mode p, this condition requires that

$$\int f_p(y)\psi_L(x_0,y)dy=\int f_p(y)\psi(x_0,y)dy. \tag{13}$$

A discrete approximation to the right-hand integral gives

$$B_p\approx\Delta\sum_{k=1}^{K}f_p(y_k)\psi_{0,k}-A\delta_{lp}, \tag{14}$$

where the summation is over the K points along the interface. Differentiating Eq. (12) with respect to x and substituting Eq. (14) for each B_r gives

$$\frac{\partial\psi_L(x_0,y_j)}{\partial x}\approx 2i\beta_l A f_l(y_j)-i\Delta\sum_{k=1}^{K}\psi_{0,k}\sum_{r=1}^{R}\beta_r f_r(y_j)f_r(y_k). \tag{15}$$

At each point $(0,j)$ on the interface we approximate $\partial^2\psi/\partial x^2$ by the $O(\Delta^2)$ forward difference equation

$$\frac{\partial^2\psi_{0,j}}{\partial x^2}\approx\frac{2}{\Delta}\left[\frac{\psi_{1,j}-\psi_{0,j}}{\Delta}-\frac{\partial\psi_{0,j}}{\partial x}\right]. \tag{16}$$

Since the first derivative of ψ must be continuous at x_0, $\partial\psi_{0,j}/\partial x=\partial\psi_L(x_0,y_j)/\partial x$. Consequently Eq. (15) can be used to approximate the first derivative in Eq. (16). Adding Eq. (4) gives an $O(\Delta^2)$ expression for $\nabla^2\psi$ that involves only known constants and the wave function values at points on and immediately to the right of the interface. A discrete approximation to Eq. (1) can then be obtained for each interface point and substituted into Eq. (5). The use of Eq. (16), which is second-order accurate, at the interface has a negligible effect on the accuracy of the solution provided that $K\ll N$.

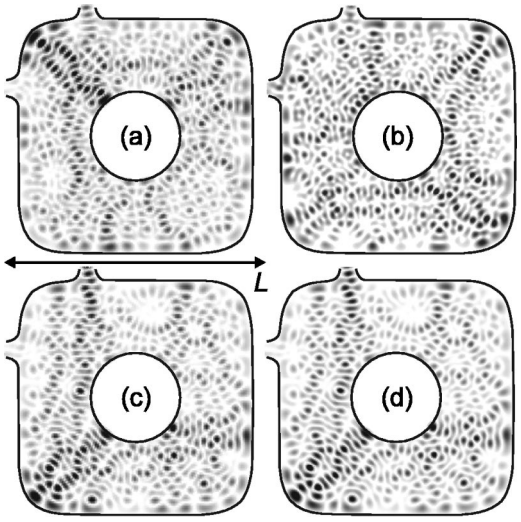

FIG. 4. Probability density plots (black high, white 0) for an electron in a 2D quantum dot calculated using (a) and (b) the $O(\Delta^2)$ and (c) and (d) the $O(\Delta^4)$ methods. Solid curves show equipotentials at the Fermi energy. In (a) and (c) $\Delta=L/255$ and in (b) and (d) $\Delta=L/349$ where $L=1$ μm.

To demonstrate the enhanced convergence of our $O(\Delta^4)$ method, Fig. 4 shows the probability density of an electron at the Fermi energy (8.2 meV) in a quantum dot. The dot has a smooth 2D potential profile that generates classically chaotic electron dynamics [6]. Two semi-infinite leads are attached to the dot, the injection lead is connected to the upper quantum point contact (QPC) opening, and the exit lead to the left-hand QPC opening. In these calculations, ten modes [$R=10$ in Eq. (12)] were required in each lead to give good convergence. The lowest two of these modes were propagating, the other eight were evanescent. Figures 4(a) and 4(b) show probability density plots calculated using the $O(\Delta^2)$ method. In Fig. 4(a) there are 254 points along each side of the dot, while in Fig. 4(b) there are 348 points along each side. Since changing the number of points changes the resulting wave function, it is clear that these calculations have not converged. By contrast, Figs. 4(c) and 4(d) show similar plots calculated using the $O(\Delta^4)$ method. The convergence of this technique is clearly superior to that of the $O(\Delta^2)$ method, as there is no change between Fig. 4(c) (254 points per side) and Fig. 4(d) (348 points per side).

In conclusion, we have introduced a general compact fourth-order FD method for solving 2D PDEs. Using this technique, Dirichlet boundary conditions can be applied on an arbitrarily shaped boundary without resorting to a stepped approximation. Our calculations for electrons in a chaotic quantum dot demonstrate that the convergence of this method is much better than that of the standard second-order technique.

This work is funded by EPSRC UK.

[1] M. Arad, A. Yakhot, and G. Ben-Dor, Int. J. Numer. Methods Fluids **23**, 367 (1996).
[2] I. Singer and E. Turkel, Comput. Methods Appl. Mech. Eng. **163**, 343 (1998).
[3] P.B. Wilkinson *et al.*, Phys. Rev. Lett. **86**, 5466 (2001).
[4] A. Taflove, *Computational Electrodynamics* (Artech, Boston, 1995).
[5] If there is an applied magnetic field, the Schrödinger equation contains first derivatives of the wave function. These can also be determined from the matrix inversion.
[6] C.R. Tench *et al.*, Physica E (Amsterdam) **7**, 726 (2000).